

# Numerical simulation of $^4\text{He}$ superfluid weak link formation in nanoaperture arrays

Tyler Volkoff,<sup>1</sup> Yongkyung Kwon,<sup>2,\*</sup> and K. Birgitta Whaley<sup>1,†</sup>

<sup>1</sup>*Berkeley Quantum Information and Computation Center and Dept. of Chemistry, UC Berkeley*

<sup>2</sup>*Division of Quantum Phases and Devices, School of Physics, Konkuk University, Seoul 143-701, Korea*

(Dated: April 4, 2014)

We present a numerical path integral Monte Carlo study of the global superfluid fraction and local superfluid density in cylindrically-symmetric reservoirs of liquid  $^4\text{He}$  separated by nanoaperture arrays. We find that in response to translations along the axis of symmetry, reservoirs separated by sufficiently small apertures exhibit suppression of global superfluid density compared to a cylinder with no intervening aperture array, for all temperatures below  $T_\lambda$ . Suppression is greatest when the aperture diameter is smaller than twice the empirical temperature-dependent  $^4\text{He}$  healing length, i.e., when the aperture has become a superfluid weak link. Increasing the diameter of a single aperture or the number of apertures in the array results in an increase of the superfluid density toward the expected bulk value. However, the total cross-sectional area of the apertures is found to not uniquely determine the superfluid density and the latter is instead seen to be dependent on the ratio of the healing length to the individual aperture radii as well as on the form of the radial atomic density. We propose and compare several different methods of estimating the length-scale of decay of superfluidity at the radial boundaries of the system through analysis of the local superfluid density distribution.

PACS numbers: 67.25.dr, 67.25.de

## I. INTRODUCTION

Unlike the case of normal-metal weak links between superconductors or weak links between reservoirs of liquid  $^3\text{He}$ , the construction of superfluid weak links between reservoirs of liquid  $^4\text{He}$  presents a considerable engineering challenge.<sup>1</sup> This is due to the difference in the orders of magnitude for the healing length,  $\xi$ , deep in the condensed phase between those BCS-type systems and liquid  $^4\text{He}$  (*e.g.*, the value of  $\xi(T=0)$  is on the order of  $1.0\ \mu\text{m}$  for a type-II BCS superconductor,<sup>2</sup>  $64\ \text{nm}$  for  $^3\text{He}$ , and  $0.3\ \text{nm}$  for  $^4\text{He}$ ). If two reservoirs of liquid helium are separated by an array of nanoapertures with average cross-sectional diameter  $10\ \text{nm}$ , normal fluid can completely fill the array to create a weak link only at temperatures  $T$  such that  $T_\lambda - T \lesssim 0.05\ \text{mK}$ , where  $T_\lambda \approx 2.17\text{K}$  is the temperature of the lambda transition.<sup>3</sup> Engineering of aperture arrays with apertures tens of angstroms in diameter would allow probing of  $^4\text{He}$  weak link formation deep in the superfluid phase.

The observation of Josephson oscillations at temperatures just below the lambda transition between reservoirs of liquid  $^4\text{He}$  separated by arrays of nanoapertures of characteristic diameter  $\sim 40\ \text{nm}$  inspires the question of whether Josephson oscillations can be observed at lower temperatures, deep in the superfluid phase. The presence of a weak link array allowing for coherent superflow is an experimental necessity for the observation of these oscillations because of the noisiness of measurements of a small mass current through an individual aperture. It has been shown theoretically using both the classical pendulum analogy for the d.c. Josephson equation and mean-field methods that the presence of multiple apertures in an array can lead to suppression of decoherence in the macroscopic phase differences across the array.<sup>4,5</sup> In addition,

a recent quantum field theoretical analysis predicts a linear scaling of the amplitude of Josephson oscillations with the number of apertures in an array.<sup>6</sup>

In this work, we use a path-integral Monte Carlo (PIMC) method to compute, locally and globally, the superfluid density of  $^4\text{He}$  reservoirs (consisting of  $N=35\text{--}123$   $^4\text{He}$  atoms inside a tube with diameter of  $\sim 20\ \text{\AA}$  and length of  $18\text{--}24\ \text{\AA}$ ) separated by nanoaperture arrays. A periodic boundary condition is imposed along the longitudinal direction, i.e., along the tube axis, to minimize finite size effects and allow for simulation of estimators of certain physical observables which require this geometry. We study the longitudinal and rotational global superfluid responses of systems containing arrays of up to five nanoapertures arranged in various spatial distributions, with characteristic aperture cross-section diameter  $3\text{--}10\ \text{\AA}$ . The specified temperatures ( $0.25\text{K} \leq T \leq 2.0\text{K}$ ) and calculated pressures ( $\sim 3.5\ \text{bar}$ , calculated with the estimator of Ref.[7]) lie well within the bulk He II superfluid phase.

In this paper, we find that the decrease of the global superfluid fraction with increasing temperature in nanoscale reservoirs of He II confined by a non-adsorbing, cylindrically symmetric external potential is governed by the formation of weak-links in the system. A weak-link is usually defined in terms of the transport dynamics of a junction between two superfluids or superconductors:<sup>8</sup> a connection between two bulk superfluids is a weak link if the mass supercurrent through the connection in response to an external field (*e.g.*, mechanical driving in superfluids, voltage bias in superconductors) is much smaller than the response of the bulk supercurrent. A generic weak link consists of two condensed fluids separated by a junction consisting of noncondensed matter, *e.g.*, the same fluid in a noncondensed phase. Because

the superfluid mass-current density depends linearly on the superfluid density, the suppression of the superfluid density in an aperture array system below the expected bulk value is thus an indicator of weak link formation.

More specifically, an increase in the length scale characterizing the decay of superfluid density, *i.e.* an increase in the healing length, provides a mechanism for the formation of a weak link between aperture-connected reservoirs of superfluid as  $T$  increases towards  $T_\lambda$  from an initial temperature well below this. The mechanism is as follows: when the healing length scale becomes of the order of the aperture radius, the superfluid mass density does not reach its maximum value in the aperture. Hence there cannot be a mass current through the aperture without some dissipation through normal fluid flow. In the case of a weakly-interacting Bose gas below  $T_{\text{BEC}}$ , the healing length  $\xi(T)$  is defined as the length scale characterizing the decay of the condensate density mode around a pointlike disturbance to its bulk value.<sup>9</sup> In contrast, the healing length of a spatially inhomogeneous superfluid is not uniquely defined.<sup>10</sup> The temperature dependence of a healing length for liquid  $^4\text{He}$  defined through measurements of superfluid density in  $^4\text{He}$  films flowing through a slit formed by two concentric cylinders was experimentally determined in Ref.[11]. This empirical  $\xi(T)$  is given by

$$\xi(t) = 0.34 \text{ nm}/t^{0.67} \quad (1)$$

with  $t = (1 - T/T_\lambda)$  the reduced temperature.<sup>3,11,12</sup> This scaling form has also been fit to data from geometrically constrained liquid  $^4\text{He}$ , under the assumption that the ratio of the observed superfluid density (obtained from measurement of the angular momentum of the persistent current) to the expected bulk superfluid density behaves as  $\frac{\rho_{s,\text{obs}}(T)}{\rho_{s,\text{bulk}}(T)} = 1 - 2\xi(T)/D$ , with  $D$  the width of the slit.<sup>11</sup> A healing length has also been extracted from measurements of fourth sound velocity in porous alumina under some simple physical assumptions about the pore geometry.<sup>13</sup>

However, these are not the only length scales related to the boundary induced variations in superfluid density that can be defined in a confined superfluid system. In stationary liquid  $^4\text{He}$ , a displacement length  $d$  that measures the superfluid mass displacement at an interface can be introduced as follows:<sup>14</sup> in a half space  $z \geq 0$  of  $R^3$ , with superfluid density  $\rho_s(z) = 0$  at  $z = 0$  and  $\rho_s(z) \rightarrow c = \text{const.}$  as  $z \rightarrow \infty$ , the displacement length  $d$  is the length satisfying  $\int_{R^3} c\theta(z-d) = \int_{R^3} \rho_s(r)\theta(z)$ , where  $\rho_s(r)$  is the local superfluid distribution. This superfluid mass displacement definition of  $d$  was shown in Ref.[14] to scale near  $T_\lambda$  as the reciprocal of the (roton) energy gap.  $d$  and related notions of superfluid displacement constitute alternative measures of healing of the superfluid at a wall boundary and are much easier to compute directly from PIMC data than  $\xi(T)$  as it is defined in Ref.[11].

In the general context of liquid  $^4\text{He}$  in a compact, connected space defined by an irregular external poten-

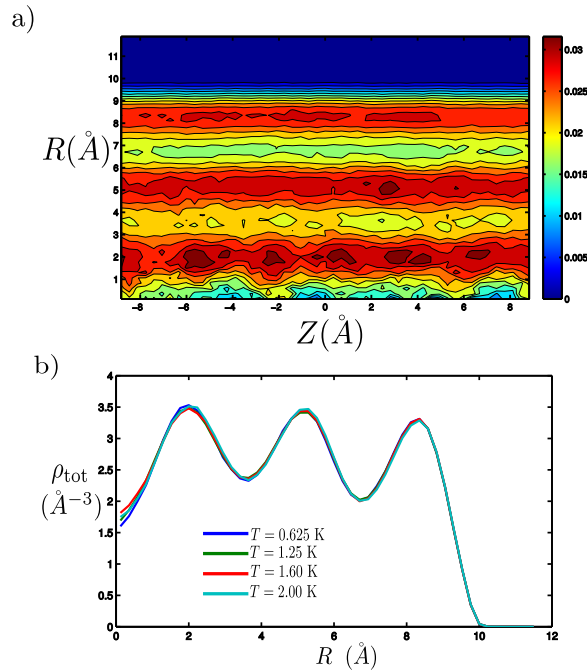


FIG. 1: 2-D density distributions of  $^4\text{He}$  atoms at  $T = 1.25\text{K}$  contained inside a tube of radius  $R_t = 10 \text{ \AA}$  and length  $L = 18 \text{ \AA}$ , with periodic boundary conditions along  $Z$ . (a) Atomic density distribution averaged over the azimuthal angle  $\phi$  (red: high density, blue: low density), computed at  $T = 1.25 \text{ K}$  (units of  $\text{\AA}^{-3}$ ). (b) One-dimensional density distribution in (units of  $\text{\AA}^{-3}$ ) computed as a function of  $R$  for a range of temperatures below the bulk  $T_\lambda \approx 2.17 \text{ K}$ .

tial, these definitions of length scales characterizing the decay of superfluid density at the boundaries must be generalized by introducing the notion of a “healing surface”. For example, in cylindrically symmetric systems parameterized by height  $Z$  and variable cylinder radius  $R(Z)$  such as we consider in this work (where  $R$  is the radial coordinate from the central guiding axis of the cylinder) a useful definition of healing surface is given by the local displacement length  $d(Z)$ , where  $d(Z) = R_t(Z) - \max \{d : R < d \Rightarrow \rho_s(R, Z) \geq 0.9f(Z)\}$ , with  $f(Z) := \max_R \rho_s(R, Z)$  and the local superfluid density is  $\rho_s(R, Z) = (1/2\pi) \int_0^{2\pi} d\phi \rho_s(R, Z, \phi)$ . The nonexistence of a positive value of  $d(Z)$  at a given cross-section ( $d(Z) = 0$ ) can then be taken as indication of the presence of a weak link. We analyze this definition of local displacement length together with other definitions in a cylinder containing no intervening aperture array at various temperatures below the bulk lambda point in Section II, and then with respect to different aperture array geometries in Section III.

## II. PIMC CALCULATIONS FOR CYLINDER GEOMETRY

For our PIMC study of  $^4\text{He}$  atoms contained in a nanoscale tube, we use the  $^4\text{He}$ -tube potential described

by:

$$V_{\text{tube}}(R, \phi, Z) = \frac{V_0}{2} \left[ 1 + \tanh \left( \frac{R - R_t}{\sigma_R} \right) \right], \quad (2)$$

where the cylindrical coordinates  $R$ ,  $\phi$ , and  $Z$  represent the distance from the tube center, the azimuthal angle, and the coordinates along the tube axis, respectively. Here  $V_0$  (potential strength) and  $\sigma_R$  (steepness of potential) are set to be 150 K and 0.25 Å. For the  $^4\text{He}$ - $^4\text{He}$  interaction, we use a well-known Aziz potential.<sup>15</sup> In the path-integral representation, the thermal density matrix at a low temperature  $T$  is expressed as a convolution of  $M$  high-temperature density matrices with an imaginary time step  $\tau = (Mk_B T)^{-1}$ . In the high-temperature density matrix the  $^4\text{He}$ - $^4\text{He}$  potentials are incorporated with the pair-product form of the exact two-body density matrices while the  $^4\text{He}$ -tube interaction in Eq. (2) is analyzed within the primitive approximation.<sup>7</sup> We use a time step of  $\tau^{-1}/k_B = 40$  K and periodic boundary conditions are imposed in the  $Z$  direction to minimize finite size effects.

We first computed the density distributions of  $N = 123$   $^4\text{He}$  atoms contained by the tube potential of Eq. (2). Figure 1(a) shows a contour plot of the density distribution at  $T = 1.25$  K averaged over the azimuthal angle  $\phi$ , with the tube radius  $R_t$  set to be 10 Å and length  $L = 18$  Å. One can observe a layering structure around the tube axis ( $R = 0$ ). Recently Kulchytskyy *et al.* performed PIMC calculations for  $^4\text{He}$  atoms inside an amorphous  $\text{Si}_3\text{N}_4$  nanopore to investigate the Luttinger liquid behaviour of a quasi-one-dimensional quantum fluid.<sup>16</sup> They found that the helium density distribution exhibited a series of cylindrical shells or layers around the pore axis, similar to that observed in Fig. 1. The layered structures for  $^4\text{He}$  inside the nanopore were understood to be due to the interplay of the  $^4\text{He}$ - $^4\text{He}$  interaction and the van der Waals interactions of  $^4\text{He}$  atoms with the pore wall. The latter interaction provided attractive adsorption sites for  $^4\text{He}$  in the vicinity of the wall and caused two outermost  $^4\text{He}$  layers to be solidified without any contribution to superfluidity at low temperatures.

Noting that the lowest value of the tube potential of Eq. (2) occurs at the center of the tube ( $R = 0$ ) and that  $V_{\text{tube}}$  increases monotonically as  $R$  increases, we understand that unlike in the situation of Ref. [16], the layering shown in Fig. 1 is due to the interparticle interaction between  $^4\text{He}$  atoms confined inside a nanoscale tube, rather than to the interaction of  $^4\text{He}$  atoms with the tube wall. Figure 1(b) shows the one-dimensional density distributions computed as a function of radius  $R$ , for several temperatures between 0.625 K and 2 K.

It is evident that there is no thermal effect on the  $^4\text{He}$  density distribution at temperatures below 2 K. The longitudinal global superfluid fraction along the tube axis, i.e., the  $Z$ -axis, may be computed by using the winding number estimator:<sup>7</sup>

$$\left( \frac{\rho_s}{\rho} \right)_z = \frac{mL^2 \langle W_z^2 \rangle}{\hbar^2 \beta N}, \quad (3)$$

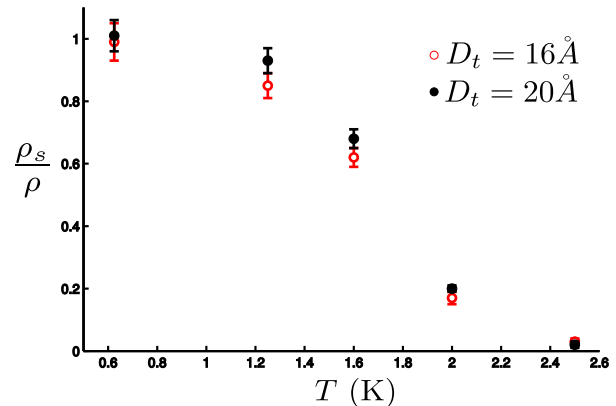


FIG. 2: (color online) Global superfluid fraction of  $^4\text{He}$  fluid contained inside tubes of diameter  $D_t = 16$  Å (open circles) and  $D_t = 20$  Å (filled circles) as a function of temperature. The calculations were made for  $N = 80$  atoms (open circles) or  $N = 123$  atoms (filled circles) in a cylinder of length  $L = 18$  Å, with periodic boundary conditions in  $Z$ .

where  $m$ ,  $L$ , and  $N$  are the bare mass of a  $^4\text{He}$  atom, the length of the tube, and the number of helium atoms inside the tube, respectively. Here the winding number  $W$  is defined by  $W_z = 1/L \sum_{i=1}^N \sum_{k=1}^M (z_{i,k+1} - z_{i,k})$ , where  $M$  is the number of time slices in the discrete path-integral representation, the sums are over particle index  $i$  and imaginary-time slice index  $k$ , and  $z_{i,k}$  is the projection of the bead position  $r_{i,k}$  onto the cylinder axis.

Figure 2 shows the global superfluid fractions of liquid  $^4\text{He}$  inside tubes with two different diameters,  $D_t = 2R_t$ , as a function of temperature. Both  $^4\text{He}$  systems are seen to show complete superfluid response below 1.25 K, as expected for bulk liquid  $^4\text{He}$ . On the other hand, the PIMC calculations of Ref. [16] for  $^4\text{He}$  atoms in a  $\text{Si}_3\text{N}_4$  nanopore showed a saturated superfluid fraction of only  $\rho_s/\rho \sim 0.2$  for  $T \lesssim 1$  K, which was understood to be due to the presence of the inert solid layers adsorbed on the pore wall. Our result showing complete superfluid response for the present  $^4\text{He}$ -nanotube system at the lowest temperatures ( $T \leq 0.625$  K) can be considered (in a general sense) as due to the fact that in contrast to Ref. [16], the tube potential of Eq. (2) does not adsorb layers of solid  $^4\text{He}$ . From a hydrodynamic perspective, lack of short-range van der Waals attraction to the boundary means there is no entrainment of the liquid helium as normal fluid, so the mass fraction of the liquid participating in superflow is higher. Alternatively, from a classical (3+1)-D theoretical perspective, an attractive van der Waals interaction with the boundary pins imaginary-time polymers, making it unlikely for the Metropolis algorithm sampling the imaginary time path integral to accept a permutation move creating an extended polymer (and thereby contributing to the winding number in Eq. (3)).

The superfluid fraction is observed to decrease for  $T \geq 1.25$  K in both  $D_t = 16$  Å and  $D_t = 20$  Å tubes, similar to the decrease seen for bulk  $^4\text{He}$  in Ref. [7]. The similarity in the rate of decrease of global superfluid fraction for both diameters can be understood by considering

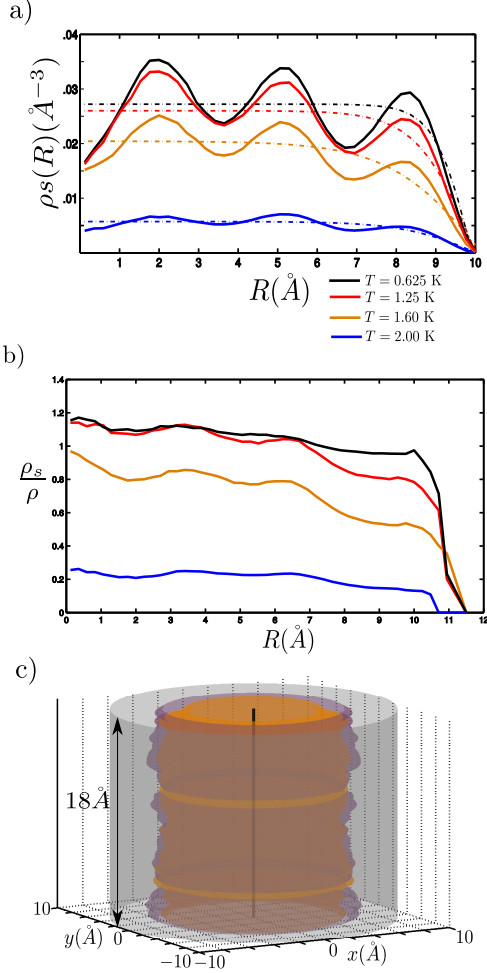


FIG. 3: (a) One-dimensional radial superfluid density distributions in a cylindrically symmetric potential for four temperatures below bulk  $T_\lambda$ . Dashed lines are least squares fits to the function  $f(R; a, b, c) = a \tanh(b(R - c))$ . The radius of the tube is  $R_t = 10 \text{ \AA}$ : calculations were made for  $N = 123$  atoms in a tube of length  $L = 18 \text{ \AA}$  with periodic boundary conditions in  $Z$ . (b) Radial superfluid fractions of liquid  $^4\text{He}$  in the same cylindrically symmetric potential as functions of radial coordinate  $R$ . (c) Healing surfaces for  $T = 0.625 \text{ K}$  (purple) and  $T = 2.00 \text{ K}$  (orange) computed using a local version of the superfluid mass displacement estimate of Method III (see text). The outer cylinder with radius  $10 \text{ \AA}$  is a guide to the eye.

the temperature-dependent global healing length  $\xi(T)$  of the superfluid. It is clear that for temperatures such that  $\xi(t) > R_t$ , the superfluid density at the center of the tube will be submaximal. The empirical formula Eq. (1) yields the following two temperature/healing length combinations for which the healing lengths are equal to half the tube diameters employed in Fig. 2:  $\xi(T = 1.56 \text{ K}) = 8 \text{ \AA}$ ,  $\xi(T = 1.74 \text{ K}) = 10 \text{ \AA}$ . Consequently, for  $T \gtrsim 1.5 \text{ K}$ , we expect that the global superfluid fraction for both  $R_t = 8 \text{ \AA}$  and  $R_t = 10 \text{ \AA}$  will be significantly suppressed below the respective maximal values: this expectation is validated by the behavior of  $\rho_s/\rho$  seen in Fig. 2.

To analyze the spatial distribution of the superfluid

density, we employ an estimator for the local superfluid density for response to translation in the  $Z$  direction that is based on the following local decomposition of the winding number estimator in Eq. (3):

$$\rho_s(\vec{r})_z = \frac{mL^2}{\hbar^2\beta} \left\langle \sum_{i=1}^{N_w} \sum_{k=1}^M \frac{W_z^2}{N_w M} \delta(\vec{r} - \vec{r}_{i,k}) \right\rangle, \quad (4)$$

where  $N_w$  is the number of  $^4\text{He}$  atoms comprising winding paths. This estimator of local superfluid density is similar to the local estimator of Khairallah and Ceperley<sup>17</sup> in the sense that all beads (*i.e.*, atoms on an imaginary-time polymer) constituting the winding paths are assumed to contribute equally to superfluidity. Although the local estimator employed by Kulchitskyy *et al.* and the one used in this work give the same proper value when integrated over space, that is, the global superfluid fraction multiplied by the total number of  $^4\text{He}$  atoms, the two estimators for the local superfluidity are based on different local decompositions of the winding number estimator (compare Eq. (4) of the present paper with Eq. (3) of Ref. [16]). Eq. (4) is locally positive semidefinite, which makes interpretation of regions of negative local superfluid density unnecessary, and also exhibits less statistical noise, making the PIMC estimation more robust.

In Figure 3, we show averages over the cylindrical coordinates  $Z$  and  $\phi$  of the radial superfluid densities,  $\rho_s(R)$ , and radial superfluid fractions,  $(\rho_s/\rho)|_R$ , computed using the local estimator of  $\rho_s(\vec{r})$  in Eq. (4). Several reasonable local and global estimators of the displacement length can be formulated from these averaged local superfluid data. To show that the radial superfluidity data exhibit healing behavior even though  $\rho_s$  does not decay monotonically in the radial direction, we propose here several methods of quantifying the length scale of the decay of superfluidity at the boundary; the corresponding numerical values are tabulated in Table I.

In Method I, a decay length is defined in terms of  $\rho_s(R)$ , by  $d := R_t - R_{\max}$ , where  $R_{\max}$  is the largest radius for which  $\rho_s(R) \geq 0.9 \max_{0 \leq R \leq R_t} \rho_s(R)$ , with  $\max_R \rho_s(R)$  being the maximum value of  $\rho_s(R)$ . Method II is a local version of Method I, where  $R_{\max}(Z)$  is now found at each point of the cylinder axis  $Z$  and  $\xi$  is the average of value of  $\xi(Z) = R_t - R_{\max}(Z)$ . Method III is an application of the “superfluid mass displacement” definition discussed in the Introduction. For each cylindrical coordinate  $Z$ , we seek  $D(Z)$  such that

$$\left( \max_{0 \leq R \leq R_t} \rho_s(R, Z) \right) \cdot D(Z) = \int_0^{R_t} dR \rho_s(R, Z) \quad (5)$$

is satisfied. In practice, the right hand side of this equation is evaluated by trapezoid rule integration of the spatially discrete  $\rho_s(R, Z)$  data obtained by integrating  $\rho_s(\vec{r})$  over  $\phi$ . The distance  $R_t - D(Z)$  is then averaged over  $Z$  to determine a global estimate of the displacement length.

In Methods IV(a,b) we perform a least squared fit of the functional form  $f(R; a, b, c) = a \tanh(b(R - c))$  to the radial averaged  $\rho_s(R)$  data (Figure 3(a) at each  $Z$ -coordinate. If we consider a subset of  $R^3$  defined by, e.g.  $\{\vec{r} = (x, y, z) | z \geq 0\}$ , the function  $f(z)$  is a solution to the Gross-Pitaevskii equation.<sup>18</sup> Note that  $f$  is a macroscopic order parameter for a weakly-interacting Bose-Einstein condensate and does not describe *a priori* the superfluid phase of liquid  $^4\text{He}$ ; it is nevertheless useful to use this functional fit to the radial superfluid density in order to show that the radial oscillations in the total and superfluid densities deriving from the interatomic interactions do not completely obscure the displacement of superfluid density from the boundary. Averaging over the values of  $b$  along the cylinder axis to get  $\bar{b}$ , a global displacement length can then be defined by  $\xi := 1/\bar{b}\sqrt{2}$  (Method IV(a)) and an effective condensate density can be defined by  $n_0 := \sqrt{\bar{a}}$  (also tabulated in Table I for the given temperatures). Instead of defining  $d$  directly from  $\bar{b}$ , we may choose to define it as the average distance from the cylinder wall at which  $f(R)$  obtains 90% of its maximum value (Method IV(b)).

Methods III and IV(a,b) are the only methods which average out the observed radial oscillations. In Section III, we apply Method III for calculating the displacement length in a system consisting of a superfluid reservoir interrupted by an aperture array.

Methods II, III, IV(a,b) can be used to construct cylindrically symmetric healing surfaces because they can be carried out at each point on the cylinder axis. The estimated healing surface obtained using Method III is shown in Figure 3 (c). We do not expect the bulk scaling of Eq.(1) near the lambda point to be applicable to the displacement length estimators in the confined liquid considered in this paper, due to finite size effects and the long wavelength cutoff imposed by the external potential (as  $R_t$ ); in particular,  $\lim_{T \rightarrow T_\lambda^-} d(T) = \infty$  is not expected in our simulations, rather,  $d(T)$  should remain a smooth function in any neighborhood of the lambda point. Thus, for all displacement length measures considered here, we see a smaller rate of increase of  $d(T)$  for low  $T$  than is expected from Eq.(1) for  $\xi(T)$ . We note that the displacement length from a planar boundary calculated from the free energy of the Hills-Roberts theory<sup>19</sup> also increases more slowly with temperature than the empirical healing length.

### III. PIMC CALCULATIONS FOR CYLINDRICAL RESERVOIRS SEPARATED BY AN APERTURE ARRAY

An analysis of global superfluid fraction and local superfluid density may be undertaken for reservoirs of liquid  $^4\text{He}$  separated by a septum pierced with one or more apertures; a cross-sectional view of a single aperture in the septum is shown in Fig. 4(a). The external potential

TABLE I: Decay lengths  $d(\text{\AA})$  of liquid  $^4\text{He}$  subject to the one-body potential in Eq.(2) calculated from radial local superfluid density according to Methods I - IV (see text for detailed descriptions). The empirical healing length, Eq. (1) is given in the first column. The sixth column is the effective global condensate density estimate obtained at a given  $T$  from the least squares fit of a Gross-Pitaevskii equation solution to the radial superfluid density  $\rho_s(R)$ .

	Eq.(1)	I	II	III	IV(a)	IV(b)	$n_0$
$T = 0.625$ K	4.27	5.41	6.32	3.84	1.33	3.33	0.17
$T = 1.25$ K	6.04	5.88	7.23	3.98	1.61	3.83	0.16
$T = 1.60$ K	8.33	6.12	7.58	4.13	1.99	4.57	0.14
$T = 2.00$ K	18.73	5.41	6.72	4.27	1.76	4.10	0.08

due to the boundary in this case described by

$$V_{\text{wall}}(R, \phi, Z) = \frac{V_0}{2} \left[ 1 + \tanh\left(\frac{R - R_t}{\sigma_R}\right) \right] + \frac{V_0}{8} \left[ 1 + \tanh\left(\frac{Z + \delta}{\sigma_Z}\right) \right] \left[ 1 - \tanh\left(\frac{Z - \delta}{\sigma_Z}\right) \right] \left[ 1 + \tanh\left(\frac{R - R_a}{\sigma_R}\right) \right], \quad (6)$$

with the following parameters (set equal to the specified fixed values if they are held constant in the simulations):

- 1) maximum potential strength:  $V_0 = 150$  K,
- 2) tube radius:  $R_t$
- 3) tube length:  $L$
- 3) steepness of potential at cylinder boundary:  $\sigma_R = 0.2 \text{ \AA}$ ,
- 4) septum thickness:  $2\delta$ ,
- 5) steepness of potential at septum boundary:  $\sigma_Z = 0.2 \text{ \AA}$ ,
- 6) aperture radius:  $R_a = D_a/2$ .

We first computed the superfluid fraction in a system of  $N = 35$  atoms with a single intervening aperture of various diameters  $D_a$  (Fig. 4 (b)). Here the aperture center coincides with the center of the septum (both on the cylinder axis). At both  $T = 0.625$  K and  $T = 1.25$  K, no superflow is observed through apertures with diameters less than  $3 \text{ \AA}$ . As the aperture diameter is increased, the superfluid fraction increases to reach the values corresponding to those of reservoirs without a septum (see Fig. 2). At  $T = 0.625$  K, the simulations show non-negligible superflow through the hole with diameter larger than  $4 \text{ \AA}$  while the diameter of the aperture should be larger than  $\sim 5 \text{ \AA}$  to observe significant superfluid fraction at  $T = 1.25$  K. The empirical healing length of the  $^4\text{He}$  fluid at  $T = 0.625$  K and  $T = 1.25$  K are calculated from Eq.(1) to be  $4.27 \text{ \AA}$  and  $6.04 \text{ \AA}$ , respectively. Our data shows that  $\rho_s/\rho$  is suppressed below unity for either temperature when their respective aperture diameters satisfy  $D_a \lesssim 2\xi(T)$ , which is consistent with weak link behavior. Conversely, for  $D_a$  larger than  $2\xi(T = 0.625 \text{ K})$ , the superfluid fraction reaches unity (within statistical error), see Fig.4 (b).

In Fig. 4 (c), we show (black filled squares) the global superfluid fraction of liquid  $^4\text{He}$  reservoirs composed in total of  $N = 90$  atoms connected by arrays of  $N_a =$



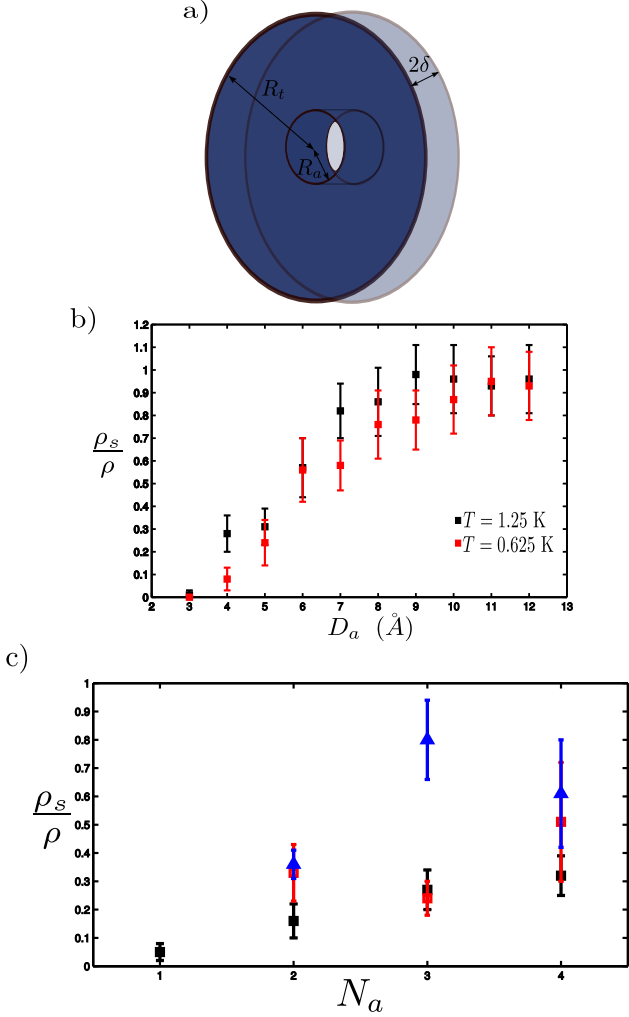


FIG. 4: (color online) a) Cross-sectional view of a single aperture in a septum separating cylindrical reservoirs of liquid  $^4\text{He}$  with  $D_t = 13$  Å. b) Superfluid fraction of reservoirs ( $D_t = 13$  Å,  $L = 24$  Å) of liquid  $^4\text{He}$  connected by a single atomic-scale aperture as a function of aperture diameter at temperatures  $T = 0.625$  K (black squares) and  $1.25$  K (red squares). c) Global superfluid fraction of  $^4\text{He}$  reservoirs ( $D_t = 20$  Å,  $L = 24$  Å) connected by multiple apertures of atomic dimensions at  $T = 0.625$  K: (black filled squares)  $\rho_s/\rho$  for arrays with  $D_a = 5$  Å as a function of  $N_a$ , the number of the apertures; (red filled squares) on-axis aperture, area-equivalent to the  $N_a$ -aperture array; (blue triangles) 1 Å off-axis aperture, area-equivalent to the  $N_a$ -aperture array. All the apertures are of the same thickness  $2\delta = 3$  Å and all calculations use periodic boundary conditions in  $Z$ .

1, 2, 3, 4 apertures where all apertures have the same diameter,  $D_a \equiv 2R_a = 5$  Å and their centers are equiangularly distributed on a circumference of  $R = 4$  Å from the tube axis. As expected, the superfluid fraction is seen to increase with  $N_a$ . However this increase is not simply determined by the total cross-sectional area of all apertures. We test this by comparing the results of calculations of single intervening apertures having equivalent total area to the  $N_a = 2, 3, 4$  aperture arrays, respectively, to this data. The red and blue symbols in

Fig. 4 c) show the superfluid fraction for area-equivalent apertures located on axis (red squares) and off axis by 1 Å (blue triangles). It is evident that reservoirs with a single interrupting aperture having the same total cross-sectional area as an aperture array with  $N_a = 2, 3, 4$  can exhibit a different global longitudinal superfluid fraction from the area-equivalent array, implying that the total cross-sectional area of the apertures does not uniquely determine the temperature-dependent global superfluid fraction  $\rho_s/\rho$ .

We find that two factors influence this interesting feature, namely the displacement of the single aperture from the cylinder axis, and the diameter of the single aperture relative to the temperature-dependent empirical healing length in Eq.(1). For the latter consideration, note that  $5 \text{ Å} > \xi(T = 0.625\text{K}) > 2.5 \text{ Å}$ . The left hand side of this inequality is the radius of a single aperture which is area-equivalent to four apertures with  $R_a = 2.5$  Å each. It is clear from the  $N_a = 4$  column of Fig. 4 (c) that at  $T = 0.625\text{K}$ , a single aperture with  $R_a = 5$  Å that is displaced 1 Å off the cylinder axis exhibits much larger  $\rho_s/\rho$  than an area-equivalent 4-aperture array ( $R_a = 2.5$  Å for each individual aperture). On the other hand, the  $N_a = 2$  column shows that a single aperture with  $R_a = 5/\sqrt{2} \text{ Å} < \xi(T = 0.625\text{K})$ , which has the same total cross-sectional area as an array of two apertures, each with  $R_a = 2.5$  Å, does not exhibit such a large increase in global longitudinal superfluid fraction, whether it is located on- or off-axis. We explain this difference by invoking our notion of a weak link as a connection which has a characteristic radius smaller than the empirical healing length at a given temperature. In the present example, while all apertures in both  $N_a = 2$  and  $N_a = 4$  are weak links, the area-equivalent single aperture centered 1 Å off-axis for the  $N_a = 4$  aperture array is not a weak link ( $R_a > \xi(T)$ ), while the analogous single area-equivalent aperture for the  $N_a = 2$  array is a weak link ( $R_a < \xi(T)$ ). The area-equivalent aperture for the  $N_a = 4$  array allows for strong coupling between the reservoirs and thus can support greater superfluid flow across the septum.

However, it is also evident that consideration of the ratio  $\xi(T)/R_a$  does not suffice to explain the dependence of this difference in  $\rho_s/\rho$  between an aperture array and its area-equivalent single aperture on the radial coordinate, on the displacement of the single aperture center from the cylinder axis (Fig. 4c)). This dependence is especially evident for the single apertures area-equivalent to the two largest,  $N_a = 3$  and  $N_a = 4$ , aperture arrays. In particular, for  $N_a = 4$ , the on-axis area-equivalent aperture (red square) shows a considerably smaller increase in  $\rho_s/\rho$  than the 1 Å off-axis area-equivalent aperture. For  $N_a = 3$ , the radius of the area-equivalent single aperture is very close to  $\xi(T = 0.625\text{K})$  and so this case must be considered as intermediate between the independence of superfluid fraction increase on area-equivalent single aperture location seen for  $N_a = 2$  and the strong dependence on this location for  $N_a = 4$ . We ascribe the

dependence of the increase in  $\rho_s/\rho$  for an area-equivalent single aperture on its position within the septum to the inhomogeneity of the radial atomic density due to the confining potential (see, e.g. Fig.1b.) It is clear that the radial density of atoms at 1 Å from the cylinder axis is greater than the density on the cylinder axis; we therefore expect that the same system with a 2 Å off-axis aperture, which is centered at a radius with relatively high atomic density, should exhibit a larger global superfluid fraction. The relative weights of the contributions of healing and inhomogeneous atomic density to the global superfluid density of a weak link separating nanoscale superfluid reservoirs merits further study.

The suppression of global superfluid response to translations along the cylinder axis is due to solely to the intervening aperture array. This is illustrated in Figure 5 a) by comparison with the estimator of global superfluid response to rotation about the cylinder axis, which can be written in terms of the mean squared projected areas of imaginary-time polymers on the plane perpendicular to that axis:<sup>7</sup>

$$\left(\frac{\rho_s}{\rho}\right)_z = \frac{2mT\langle A_z^2 \rangle}{\lambda I_c}. \quad (7)$$

Here  $A_z = \frac{1}{2}P_z \sum_{\ell=1}^N \sum_{j=1}^{\beta/\tau} r_{\ell,j} \times r_{\ell,j+1}$  is the vector area directed along  $\hat{z}$ , with magnitude equal to the polymer area projected onto the  $R, \phi$  plane ( $P_i$  is the projection of the vector area onto the  $i$  axis),  $\lambda := \hbar^2/2m$ , and  $I_c = \langle \sum_{\ell=1}^N \sum_{j=1}^{\beta/\tau} m(r_{\ell,j} - P_z r_{\ell,j}) \cdot (r_{\ell,j+1} - P_z r_{\ell,j+1}) \rangle$ . Evaluating the projected area estimator along the cylinder axis gives the upper traces in Fig. 5 a) (square symbols). The rotational response is consistently larger than the translational response (lower traces, triangular symbols) and also shows saturation of global superfluid response for low  $T$ , whereas the translational response shows only a small increase at lower temperatures and remains less than 0.4 for all temperatures studied. This difference reflects the fact that the rotational response about the cylinder axis is determined primarily by rotation in the tube away from the septum and is not significantly affected by the presence of weak links within the septum. The latter reduce the translational flow along the axis and thus significantly reduce the translation response along this axis. To further probe this difference, we report in Fig. 5 calculations for two locations of the aperture (red symbols for on-axis and black symbols for 4 Å off-axis). Within statistical error, it appears that neither the global superfluid fraction for rotational response (upper traces) nor that for the translational response (lower traces) are significantly affected by the position of the aperture in the array. This is consistent with the above analysis of the translational response being determined by a weak link, independent of the aperture position, while the rotational response is largely independent of both the septum and aperture structure. Indeed, calculation of the displacement length by the Method III introduced in Section II for the single aperture systems in Fig. 5 a) shows that, in addition to the empirical healing

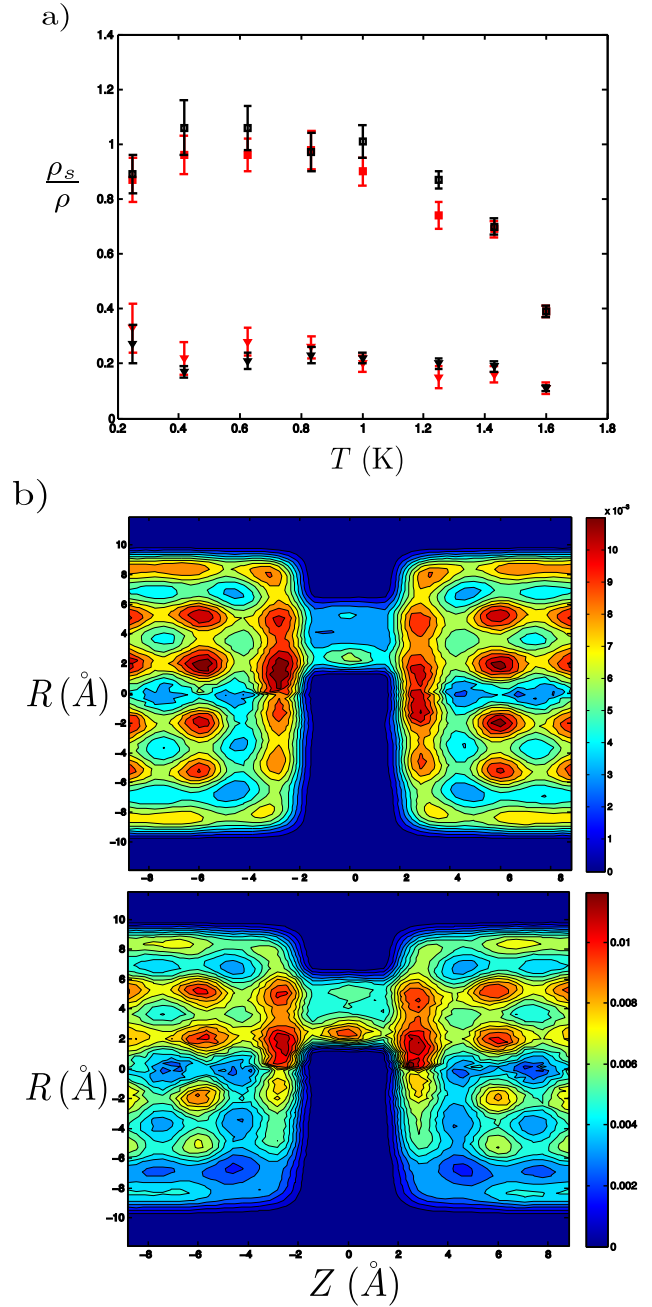


FIG. 5: a) Comparison of global superfluid fraction for response to rotation about the cylinder axis, computed by the projected path area estimator in Eq. (7) (squares) with the superfluid fraction for response to translation along the cylinder axis, computed by the winding number estimator (inverted triangles), for reservoirs of  $^4\text{He}$  ( $N = 100$ ) separated by a septum containing a single aperture with  $\delta = 1.5$  Å and  $D_a = 6$  Å. Red symbols denote results with the aperture on-axis, black symbols results with the aperture off-axis by 4 Å.) b) Local superfluid densities  $\rho_s(Z, R)$  for response to translation along the cylinder axis (obtained by averaging Eq.(4) over the angular coordinate  $\phi$ ), shown as functions of  $(Z, R)$  in cylinders with a single off-center aperture having  $\delta = 1.5$  and  $D_a = 6$  Å at  $T = 0.25$ K (top) and  $T = 1.00$ K (bottom).

TABLE II: Displacement lengths ( $\text{\AA}$ ) of liquid  $^4\text{He}$  subject to the one-body potential in Eq.(6) calculated by Method III from Section II.

$T$ (K)	0.250	0.417	0.625	0.833	1.000	1.250	1.430	1.600	2.000
$d(T)(\text{\AA})$	4.39	4.62	4.78	4.95	4.98	5.34	5.42	5.93	6.38

length, the displacement length is greater than the aperture radius for all temperatures studied (Table II). This is consistent with weak-link formation due to suppression of superfluidity in the aperture and confirms the validity of our explanations for the difference between the rotational and translational response, as well as the lack of dependence of the latter on the location of the aperture center.

In the case of an off-axis aperture, it is clear from Fig. 5 (b) that the displacement length estimators introduced in Section II are ambiguous; the superfluid density decays with a different characteristic length in the half-cylinder containing the aperture from that in the half-cylinder without it. As a consequence, healing surfaces as computed by Methods II, III, and IV(a,b) in Section II are asymmetric about the cylinder axis. These results show that the superfluid mass density may be displaced asymmetrically from the boundaries in a manner which depends on the geometry of the confining potential. Global estimates of healing behavior cannot account for the asymmetry; this is why the introduction of the notion of a healing surface, which reveals the local structure of healing, is necessary.

#### IV. SUMMARY AND CONCLUSIONS

We have used PIMC numerical simulation to analyze the formation of weak links in cylindrically-symmetric reservoirs of liquid  $^4\text{He}$  with and without a bisecting array of microscopic apertures, using an external potential for the  $^4\text{He}$  reservoirs that precludes adsorption at the boundary. Global superfluid fractions measuring response to translational motion along the cylinder axis have been calculated for these systems as functions of temperature, number of apertures in an array, and aperture radius, by using the estimator in Eq.(3) that is based on the on-axis winding number of imaginary-time polymers. We have proposed four definitions of decay length  $d$  for inhomogeneous helium superfluid densities at a boundary which can be readily evaluated using PIMC simulation of a positive-definite estimator (Eq.(4)) of local superfluid density that weighs all beads participating in on-axis winding paths equally. Each of these definitions can be used to define a global length scale of the decay in superfluid density at the boundary of the cylinder, while three of them (II, III and IV) can be used to construct healing surfaces that reveal local variations in the decay of helium density along the cylinder boundary. In the absence of a septum and any apertures, the

superfluid decay length estimators show an increase with temperature over the range  $T = 0.625 - 1.6$  K. Because of the confined geometry and long distance cutoff imposed by the external potential, these length scales of superfluid decay do not show the singular behavior associated with the empirical temperature-dependent healing length  $\xi(T)$  of bulk  $^4\text{He}$  and also show a smaller rate of increase for low temperatures.

For a single aperture in a septum between the reservoirs, we found that suppression of the superfluid fraction in response to longitudinal ( $Z$ -axis) translation correlates with the empirical temperature-dependent healing length  $\xi(T)$  becoming of the order of the radius of the aperture, *i.e.* with the formation of a weak link in the system. Comparison of the superfluid fraction for a cylinder with septum containing an array of up to  $N_a = 4$  apertures, with the corresponding superfluid fraction for a single area-equivalent aperture, revealed interesting differences. In particular, the total cross-sectional area of the apertures in an array does not uniquely determine the global superfluid fraction. These differences could be analyzed in terms of the basic notion of a weak link as a connection between the helium reservoirs that has a characteristic radius smaller than the healing length, as well as the secondary role of inhomogeneities in the helium density due to the confining potential. Detailed analysis of the relative role of these factors for helium flow between nanoscale reservoirs via weak links constitutes an interesting topic for further study.

In systems containing an aperture array, we also calculated the global superfluid fraction for response to rotation about the cylinder axis, using an estimator, Eq.(7), based on the projected areas of the polymer paths. In contrast to the suppressed superfluid fraction in response to translational motion along the cylinder axis, very little suppression of superfluid fraction due to rotational response below the expected bulk value is observed in presence of an aperture array. This is consistent with the primary consequence of the presence of an intervening aperture array: a reduction of superfluid current along the cylinder axis. Suppression of the global superfluid fraction as measured by rotational response could be achieved by inserting an aperture array that longitudinally bisects the cylinder (instead of transversally).

For systems with a single aperture, the superfluid decay length defined according to the mass-displacement method of Ref.[14] (Method III) showed a monotonic increase in  $d(T)$  with temperature comparable to the Hills-Roberts theory for low temperature.<sup>19</sup> We found a suppression of translational response superfluid fraction in a single-aperture system with  $D_t < 2d(T)$  for  $0.25 \text{ K} < T < 2.00 \text{ K}$ . In systems containing an off-axis intervening aperture, asymmetrical displacement lengths are observed in the upper and lower halves of the cylinder. This asymmetry could be exploited in designing aperture arrays for experiments in superfluid hydrodynamics.

In this work we have considered only static proper-



ties of the constrained superfluid. In order to analyze the effects of externally imposed flow on the local superfluid density and healing lengths with PIMC, local estimators of velocity and vorticity and their correlations must be calculated. We have derived an estimator for the local vorticity in the system that will divulge information about the equilibrium structure of line-like defects in superfluid density in cylindrically confined systems. Results in this direction will be reported in a future publication.

### Acknowledgments

This work was supported by the Basic Science Research Program (2012R1A1A2006887) through the Na-

tional Research Foundation of Korea funded by the Ministry of Education, Science and Technology and by the National Science Foundation (NSF) Grant No. PH9-0803429 through the Physics at the Information Frontier Program. TJV acknowledges the NSF/NRF Korea EAPSI program for funding and H. Shin and S. Park for useful suggestions.

---

\* Electronic address: ykwon@konkuk.ac.kr

† Electronic address: whaley@berkeley.edu

<sup>1</sup> Y. Sato and R. Packard, Rep. Prog. Phys. **75**, 016401 (2012).

<sup>2</sup> T. Tsuneto, *Superconductivity and superfluidity* (Cambridge University Press, 1998).

<sup>3</sup> E. Hoskinson, Y. Sato, I. Hahn, and R. Packard, Nature Physics **2**, 23 (2006).

<sup>4</sup> D. Pekker, R. Barankov, and P. Goldbart, Phys. Rev. Lett. **98**, 175301 (2007).

<sup>5</sup> T. Chui, W. Holmes, and K. Penanen, Phys. Rev. Lett. **90**, 085301 (2003).

<sup>6</sup> T. Volkoff and K. Whaley, J. Phys.: Condens. Matter **25**, 275602 (2013).

<sup>7</sup> D. Ceperley, Rev. Mod. Phys. **67**, 279 (1995).

<sup>8</sup> K. Likharev, Rev. Mod. Phys. **51**, 101 (1979).

<sup>9</sup> H. Kleinert, *Gauge fields in condensed matter: Volume II* (World Scientific, 1989).

<sup>10</sup> R. Donnelly, *Quantized vortices in He II* (Cambridge Uni-

versity Press, 1991).

<sup>11</sup> R. Henkel, E. Smith, and J. Reppy, Phys. Rev. Lett. **23**, 1276 (1969).

<sup>12</sup> L. S. Goldner and G. Ahlers, Phys. Rev. B. **45**, 13129 (1992).

<sup>13</sup> W. Tam and G. Ahlers, Phys. Lett. A **92**, 445 (1982).

<sup>14</sup> P. Roberts, R. Hills, and R. Donnelly, Phys. Lett. **70A**, 437 (1979).

<sup>15</sup> R. Aziz, M. Slaman, A. Koide, A. Allnatt, and W. Meath, Mol. Phys. **77**, 321 (1992).

<sup>16</sup> B. Kulchitsky, G. Gervais, and A. Del Maestro, Phys. Rev. B **88**, 064512 (2013).

<sup>17</sup> S. Khairallah and D. Ceperley, Phys. Rev. Lett. **95**, 185301 (2005).

<sup>18</sup> V. Ginzburg and L. Pitaevskii, J. Exptl. Theoret. Phys. **34**, 1240 (1958).

<sup>19</sup> R. Hills and P. Roberts, Q. Jl. Mech. Appl. Math. **40**, 279 (2003).